Stress, Strain and Magnetic Anisotropy: All Is Different in Nanometer Thin Films

Dirk Sander[1], Holger Meyerheim[1], Salvador Ferrer[2], and Jürgen Kirschner[1]

[1] Max-Planck-Institut für Mikrostrukturphysik
Weinberg 2, D-06120 Halle, Germany
sander@mpi-halle.de

[2] European Synchrotron Radiation Facility
B.P. 220, F-38043 Grenoble Cedex, France

Abstract. The application of the crystal curvature technique for stress measurements at surfaces and in films is presented. Important aspects regarding sample clamping and elastic anisotropy are elucidated in view of a quantitative stress analysis. Combined stress measurements and structural characterizations are mandatory to obtain a meaningful interpretation of the stress data. The in-situ combination of surface X-ray diffraction with stress measurements indicates a previously unknown substantial distortion of a W(110) surface layer upon Ni coverage, and the decisive role of this substrate relaxation for the stress state is discussed. The magnetization-induced stress in epitaxial layers is measured to derive the magneto-elastic coupling coefficients, which drive the magnetostriction of bulk samples. It is found that even a subtle film strain in the sub-percent range leads to a drastically modified magneto-elastic coupling in the films as compared to the respective bulk value. The implication of non-bulk like magneto-elasticity for the magnetic anisotropy of strained films is emphasized, and recent progress in the theoretical description of the strain-dependent modification of the magneto-elastic coupling is acknowledged.

1 Introduction

Mechanical stress in thin films is known as one of the most important issues when it comes to the application and reliability of thin film devices [1,2,3]. A dramatic example of thin film failure is the delamination of a thin film from its substrate. G.G. Stoney described already in 1909 [4] that this failure of thin films has been observed as early as 1858, and he writes, "I have had the same experience in protecting silver films in searchlight reflectors by a film of electro-deposited copper, it being found that if the film of copper is more than 0.01 mm thick peeling is apt to take place". Stoney concluded that the Cu film was deposited under tension, which seems very plausible from today's point of view taking the different lattice constants of Cu (3.61 Å) and Ag (4.09 Å) into account. The difference of the lattice constants leads indeed to a tensile lattice misfit of +13.3 %. An example for the delamination a 900 nm Cr film under tensile stress from a glass substrate is shown in Fig. 1a.

B. Kramer (Ed.): Adv. in Solid State Phys. 43, pp. 547–561, 2003.
© Springer-Verlag Berlin Heidelberg 2003

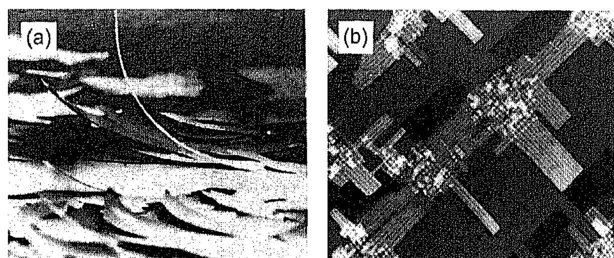

Fig. 1. Stress effects in strained films. (**a**) Delamination of a 900 nm Cr film from a glass substrate [5]. Image width 1.2 mm.(**b**) Distortion lines (*white*) in the 5th layer of Fe (*grey*), deposited on an extended four layer thin Fe film (*dark grey*) on W(001) [6]. Scanning tunneling microscopy image, image width 200 nm

The original work by Stoney [4] does not only describe the delamination phenomenon, but it also offers the first quantitative measurement of Ni-film stress from the bending of a thin steel substrate. Stoney deduced a stress of 0.3 GPa for a 5 μm thin film deposited on a steel ruler. He derived a relation – the so-called Stoney equation – between the radius of curvature R of a substrate of thickness d due to the force per unit width exerted by a film of thickness t under a stress of τ, $\tau t = Ed^2/(6R)$, with E : modulus of elasticity of the substrate. However, this relation is faulty as it neglects the two-dimensional nature of the stress and bending problem, and in the proper analysis, E is replaced by $E/(1-\nu)$, which includes the Poisson ratio ν of the substrate. Important aspects regarding quantitative stress measurements are discussed in Sect. 3.

Even in films with just a few atomic layers thickness stress is an important factor which determines the atomic structure. Considerable stress in the GPa range often induces pronounced structural relaxations, which are driven by a reduction of film stress. An example is shown in Fig. 1b, where islands of the 5th layer Fe are shown as grey patches on a four layer thick Fe film, deposited on W(100) [6]. White lines in the grey patches indicate the formation of distortion lines running along the ⟨100⟩ directions which are due to the incorporation of additional Fe atoms. This process is driven by the large misfit of 10 % between Fe and W. Incorporation of additional Fe atoms along lines in the fifth layer reduces the strain [6].

The atomic processes which govern stress relaxation on the nanometer scale are of interest in their own right, but here we discuss the implications for the magnetic properties of atomic layers layers [7]. Combined studies of both film stress and magneto-elastic coupling indicate that the magneto-elastic properties of strained films deviate sharply from the respective bulk-behavior, and film strain has been identified as a decisive factor which governs the effective magneto-elastic coupling in ferromagnetic films.

This contribution offers a brief reference to work which discussed the origin of stress at surfaces and in thin films in Sect. 2. Sect. 3 focuses on ex-

perimental set-ups for stress measurements and important aspects regarding the quantitative curvature analysis are discussed there. The stress during Ag growth on a Fe whisker is discussed in Sect. 4, and examples of combined curvature and X-ray diffraction studies are presented in Sect. 5. Sect. 6 elucidates the application of curvature measurements to investigate the magneto-elastic coupling in nanometer thin ferromagnetic films.

2 Origin of Stress in Thin Films and at Surfaces

Mechanical stress in a film can be due to lattice misfit [8], crystalline coalescence [9], surface stress changes [8,10] and magnetization processes [7], to name just a few examples. We refer the reader to the references for a deeper discussion of the underlying physical principles. Possible implications of stress at interfaces and in nanometer thin structures for pattern formation, alloying, shape and structural transitions have been reviewed [11]. In the following we present a few recent results to elucidate some selected aspects of stress measurements.

3 Experimental Aspects of Stress Measurements

Forces acting in a film, which is deposited on one surface of a substrate, induce both a bending and a dilation of the substrate. The resulting relation between film forces and curvature of the substrate has been discussed [7,8,12]. The determination of film stress proceeds via a measurement of the stress-induced deflection of the film-substrate composite.

This deflection of a substrate, which is clamped at one end, a so-called cantilever substrate, is analyzed. Various techniques have been applied successfully to detect even minute deflections of the substrate, and different experimental realizations are sketched in Fig. 2.

The relation between the radius of curvature R and the deflection line of the substrate $\xi(x)$, where x is measured along the sample length is given in good approximation by $1/R = \xi''(x)$. If the deflection is measured at the end of the substrate at $x = L$, the curvature is given by $1/R = 2\xi(L)/L^2$. Note, that this relation implies that the whole substrate of length L is covered by the film homogeneously. Also, the effect of clamping on the resulting deflection is neglected, as will be discussed below. Stress measurement by analyzing the substrate deflection have been performed with high sensitivity. E.g., the substrate might form a capacitor with a reference electrode, and a stress-induced change of the capacitor plate separation can be detected with sub-Angstrom sensitivity. If one regards the substrate as a macroscopic cantilever it is obvious, that all techniques which have been applied to detect the cantilever deflections in atomic force microscopy (AFM) can be employed to detect the substrate deflection in a stress measurement.

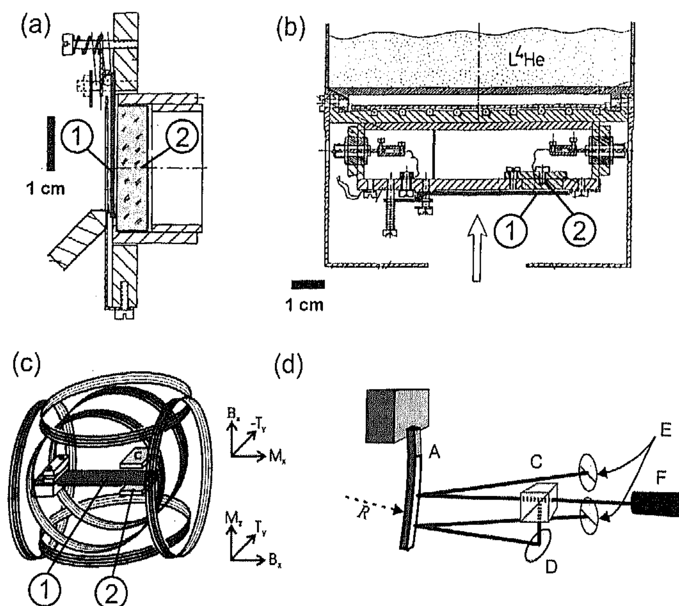

Fig. 2. Cantilever beam experiments for stress measurements. (**a**) Interferometric set-up [13]. The deflection of the cantilever 1 is detected by the change of the interference pattern produced in the gap between 1 and optical flat 2. (**b**) Capacitance measurement [14]. The deflection of the cantilever 1 induces a change of the capacitor plate distance at the position of the reference electrode 2. (**c**) Capacitance measurement with coils for magnetization measurements [15]. (**d**) Optical two beam measurement [16]. The curvature $1/R$ of the substrate A is detected by the deflection of two laser beams on the position sensitive detectors E, F. C: beamsplitter, D: mirror, F: laser

However, an important aspect with regard to quantitative stress measurements is due to the sample clamping. In most experimental situations, the thin substrate has a rectangular shape, and it is clamped along its width at one end to a sample manipulator. This clamping inhibits a curvature along the sample width near the clamping, and the resulting deflection line is considerably changed. This has been analyzed in great detail by finite-element-method calculations [17]. These calculations introduce the dimensionality of bending D, and the deviation from $D = 2$ are due to effect of clamping. The following expression describes the proper relation between curvature $1/R$ and the stress $\tau t = Yd^2/\{6(1-\nu)[(1+(2-D)\nu]R\}$, where the film thickness is given by t, and d is the sample thickness. The anisotropy of the Young modulus Y and the Poisson ratio ν of the substrate is neglected in this expression, which is a perfect approximation for W for all orientations, and also for the

(111) faces of cubic materials. In the latter case, Y and ν have to be calculated for the (111) plane [7,18].

The deviation from the ideal two-dimensional bending caused by the clamping is indicated in Fig. 3. The effect of sample clamping on the deflection line is most severe for short substrates, with an aspect ratio length/width below two. The effect of clamping is most severe when the deflection $\xi(L)$ at the sample end is measured, and it is less pronounced when the curvature $\xi''(L)$ is measured instead.

We present in Fig. 2d a two-beam optical deflection technique which allows to measure the change of slope of the substrate between two points separated along the substrate length. This difference of slope corresponds to the crystal curvature, and such a measurement resembles a curvature measurement to a good approximation. This technique has been applied to the stress measurements on a Fe whisker, which are discussed next.

We conclude by quoting typical values for the stress-induced substrate deflection. For any stress measurement of films in the nanometer thickness range, substrates thinner as 0.5 mm are mandatory. A film stress of −0.6 GPa in a 1 nm Ag film on a 0.1 mm thin Fe(001) whisker is expected to induce a radius of curvature of 570 m, the bottom end of the 10 mm long substrate will be deflected by 0.88 μm [19]. A curvature of this magnitude can be routinely detected by stress measurements. However, stress induced by magnetization processes is typically three orders of magnitude smaller, as discussed in Sect. 6, and there averaging techniques or phase-sensitive signal detection is used to increase the signal-to-noise ratio [20,21].

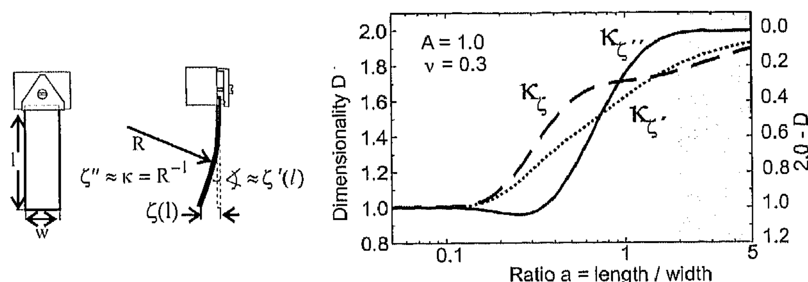

Fig. 3. Sketch of a cantilever experiment with a sample of length l and width w. The plot indicates the deviation from the true 2-dimensional bending, $D = 2$ for different aspect ratios and measurement schemes. The calculation is done for an isotropic substrate $A = 1$ with a Poisson ratio $\nu = 2$. Data from [17], with permission

4 Film Stress During Epitaxial Growth: Ag on Fe(100)

Thin single crystalline substrates are mandatory for cantilever stress measurements. For many semiconducting compounds thin samples are readily available from stock, for metals however, thicker single crystalline samples have to be polished down until the requested thickness is reached. An alternative route towards thin crystals is given by the growth of needle-like Fe whiskers from the gas phase [22]. It is well known that high quality Fe crystals can be produced, with extended (100) terraces in the μm range, which are bounded by single atomic steps. These substrates have often a square-like cross section of the order of 100 μm×100 μm, and grow in length up to 14 mm. An example of such a Fe crystal is shown in Fig. 4, and the adjacent needle indicates the small lateral dimensions of the Fe whisker. Thus, a rather thin single crystalline substrate with an exceedingly large aspect ratio $\gg 100$ is obtained, which facilitates the quantitative stress analysis due to negligible clamping effects as discussed above.

The growth of Ag on Fe(100) whiskers has been studied by reflection high energy electron diffraction (RHEED) in great detail [23,24]. RHEED oscillation of the specular intensity have been observed during the deposition at 360 K above a thickness of five Ag layers , and layer-by-layer growth has been proposed in this thickness range. The layer-by-layer growth and the small epitaxial misfit make Ag on Fe(100) an ideal prototype for stress measurements, as the resulting film stress should be given by the lattice misfit, and no stress relaxation is expected for depositions up to several dozen layers. Indeed, our measurements indicate that the stress in films above 5 layers thickness is given by the misfit, whereas surface stress effects and a possible surface alloy formation dominate the stress in thinner Ag films [19].

Between fcc Ag ($a_{Ag} = 4.08$ Å) and bcc Fe ($a_{Fe} = 2.866$ Å), the epitaxial relation is given by 45° rotated surface unit cells of the two elements. A moderate compressive in-plane lattice misfit $\eta = (a_{Fe} - a_{Ag}/\sqrt{2})/(a_{Ag}/\sqrt{2}) = -0.8$ % results. This misfit induces a biaxial film stress of $\tau = \eta Y_{Ag}/(1 - \nu_{Ag}) = -0.61$ GPa. Our stress measurements as presented in Fig. 5 confirm this magnitude of stress for layer-by-layer growth conditions for $t_{Ag} > 5$ ML.

Figure 5 shows a plot of the Ag-induced stress of the Fe(100) substrate as a function of Ag thickness in monolayers (1 ML Ag: 2.04 Å). The measurement was performed with a two-beam optical deflection technique, and the stress is

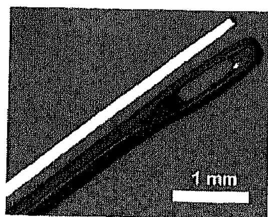

Fig. 4. Fe whisker with a mirror-like shiny surface next to a needle

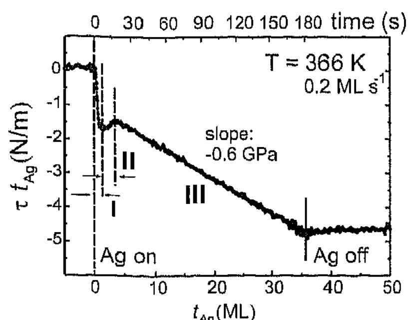

Fig. 5. Stress during Ag deposition on Fe(100), as measured on a Fe whisker (Fig. 4) with an optical two deflection technique (Fig. 2(d)). 1 ML Ag: 2.043 Å. The constant slope of the stress curve in regime III indicates a compressive stress of −0.6 GPa

deduced from the measured curvature, as described above. A negative signal indicates compressive stress, i.e. a stress, which favors an expansion of the film with respect to the substrate. Immediately after the beginning af Ag deposition, the stress drops rapidly and reaches a minimum of −1.7 N/m, after deposition of one layer Ag. Further deposition leads to a small tensile stress, and after 5 ML of deposition, the stress continues to drop, and it reaches a constant slope of −0.6 GPa. After the deposition of 35 ML Ag the Ag evaporator is closed, and the stress remains at −4.9 N/m. No significant stress relaxation is observed, and we performed additional tests to verify that a a possible radiative heating of the substrate by the Ag evaporator has no impact on the curvature measurement.

Three distinct stress regimes are identified in Fig. 5. Regime I (0–1 ML) is ascribed to the formation of the Ag-Fe interface. The measured stress change is mainly due to the relief of the tensile surface stress of Fe(100) upon coverage with Ag. The subsequent regime II (1–5 ML) is characterized by a much smaller stress change. We ascribe this to a rougher surface morphology in this thickness range, which is possibly caused by some surface alloy formation between Ag and Fe. This assumption is corroborated by the RHEED results which indicate an absence of intensity oscillations in this thickness regime [24]. Regime III (> 5 ML) is characterized by a constant slope of the stress curve given by −0.6 GPa, which is caused by the epitaxial misfit between Ag and Fe, as discussed above. We performed many stress measurements during the deposition of Ag at temperatures between 300 K and 393 K and for deposition rates between 0.05 Å/s and 0.5 Å/s, and the three stress regimes were always observed.

The back-extrapolation of the stress curve of all of our measurements from regime III to zero coverage leads to a stress value of −1.23 N/m. We ascribe this to the difference of surface stress between Ag(100) and Fe(100), and we conclude that Fe is under a larger tensile surface stress as compared to Ag. The calculated surface stress of Ag(100) is +0.82 N/m [25], and we deduce 2.05 N/m as the surface stress for clean Fe(100).

This example demonstrates that the high sensitivity of stress measurements can be exploited to investigate both adsorbate-induced changes of sur-

face stress and film stress [8]. In addition, even subtle structural relaxations, which occur during epitaxial growth, give rise to stress oscillations with a monolayer period, as has been verified for semiconductor [26] and metallic systems [16]. In conclusion, stress measurements are sensitive tools to monitor structural relaxation or composition changes at surface and in films.

An important ingredient of the stress analysis is a detailed knowledge of the atomic structure of the film-substrate composite. To this end we performed combined surface X-ray diffraction studies and curvature measurements to derive stress-strain relations at the atomic level.

5 Combined Stress and Surface X-ray Diffraction Measurements

Any interpretation of stress measurements relies on a knowledge of the geometric structure of both substrate and film. This statement might seem trivial, but we want to point out that a detailed structural investigation may reveal considerable adsorbate-induced distortions of the substrate, which cannot be anticipated, nor excluded in general. An example is presented here, where the substantial distortion of W(110) upon Ni deposition has been detected by surface X-ray diffraction [27].

In-situ combination of stress measurements with structural investigations is extremely useful. We performed such combined stress measurements by the curvature technique with surface X-ray diffraction at the beamline ID-03 of the European Synchrotron Radiation Facility (E.S.R.F.) in Grenoble, France [27,28,29,30]. The strength of combined stress and X-ray diffraction measurements is due to the high sensitivity of *both* techniques for subtle structural changes of the film-substrate composite.

A revealing example is the Nishiyama-Wassermann growth of Ni on W(110). Former investigation suggested the following sequence of Ni-structures in the first layer with increasing Ni coverage: Ni is bonded in pseudomorphic sites at small coverage, then first in a 1×8 and then in a $c(1 \times 7)$ coincidence structure [31]. These structural transitions are driven by the tendency of the Ni atoms to increase their atomic density on the W surface. These structural transitions are accompanied by a reduction of the strain along W[100] from +27 % for the pseudomorphic structure to −1.3 % for the $c(1 \times 7)$ coincidence structure. Previous low energy electron diffraction and scanning tunneling microscopy studies indicate a constant strain of +3.7 % along W[1$\bar{1}$0] [31,32]. Our recent surface X-ray diffraction studies identified the formerly proposed 1×8 coincidence structure as a structurally modulated 1×1 structure, which gives rise to satellite reflections at positions which deviate slightly from those of the former model, and a modulation period of 7.7, and not 8 lattice units, along W[100] is found by surface X-ray diffraction [27]. The proposed $c(1 \times 7)$ coincidence structure was confirmed in the recent structural analysis [27].

The c(1 × 7) coincidence structure is characterized by a coverage of 1.3 with respect to the atomic density of the W(110) surface. Only after this structure has formed, additional deposition of Ni leads to the formation of a fcc(111)-like second layer, as described by the Nishiyama-Wassermann growth mode.

The formation of the fcc(111)-like second Ni layer is accompanied by a characteristic change of the film stress from compressive c(1 × 7) coincidence structure) to tensile for the second Ni layer [27]. This demonstrates that stress measurements give an accurate and highly sensitive indication of the formation of distinct surface structures.

An example of our combined stress and surface X-ray diffraction work in shown in Fig. 6. Figure 6 shows the curvature measured along W[001] during the deposition of Ni, right axis, and the measured X-ray intensity on the left axis for a satellite reflection characteristic of the modulated 1 × 1 structure, top panel, and for the c(1 × 7) coincidence structure in the lower panel. The sequential occurrence of the two structures is revealed by the intensities of both reflections. First, the modulated 1 × 1 structure is formed, then

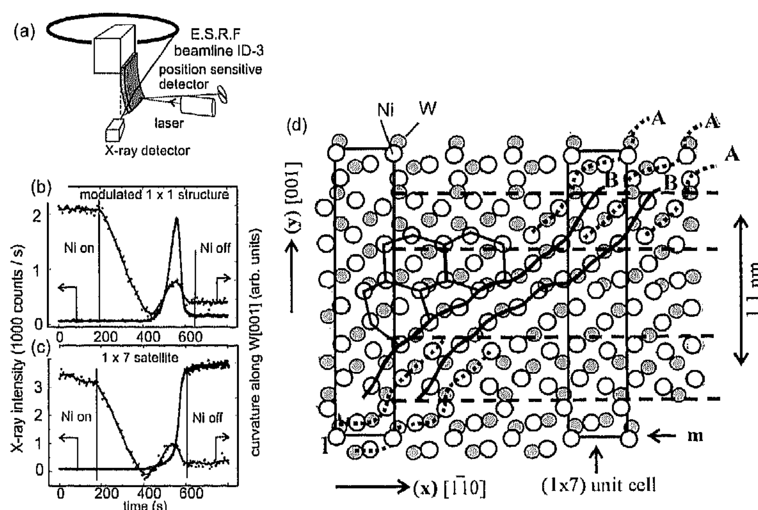

Fig. 6. Combined curvature and X-ray diffraction experiments at the ESRF. (a) Sketch of the experimental layout. Crystal curvature and diffracted X-ray intensity are measure simultaneously during Ni growth on W(110). (b) X-ray intensity (*left axis*) and crystal curvature (*right axis*) during the deposition of the first layer of Ni. The formation and disappearance of a modulated 1 × 1 structure with increasing Ni coverage coincides with the change of curvature from compressive to tensile back to compressive. (c) The 1 × 7 structure evolves only after the disappearance of the modulated structure detected in (b). (d) Structural model of the 1 × 7 structure. Atomic chains a, B between Ni and W are formed. Areas of higher atomic density are separated by 1.1 nm along [001]

its intensity drops down to almost zero with increasing deposition. While the intensity of the modulated 1×1 structure vanishes with ongoing deposition, the $c(1 \times 7)$ coincidence structure gains in intensity. The completion of the $c(1 \times 7)$ coincidence structure is identified by the vanishing slope of the curvature signal. Thus, the curvature data clearly identify the filling of the first layer, which is also characterized by the maximum diffracted intensity of the $c(1 \times 7)$ satellite. The deposition of more Ni leads to a positive slope of the curvature signal for a coverage above 1.3. The proper two dimensional stress analysis reveals that the biaxial film stress changes from compressive to tensile once the second layer Ni grows in the fcc(111)-like structure [27].

The exact Ni coverage which corresponds to the filling of the first Ni layer is identified with high precision by both techniques. The resulting $c(1 \times 7)$ coincidence structure was subsequently analyzed by surface X-ray diffraction, and the result of the structural model is presented in Fig. 6d. The main structural characteristic is the formation of atomic chains between Ni and W, as indicated by the dark lines A and B. Note, the substantial distortions of W atoms from their respective bulk positions [27].

The measured tensile stress of the second layer Ni amounts to 15 GPa, and this value can be quantitatively ascribed to an average isotropic film strain of +3.7 % [20]. We emphasize that in contrast to the thicker Ni films the stress in the first layer cannot be described by the average strain of the different structures [31]. Our X-ray investigations offer a possible cause for this complicated stress behavior of the first Ni layer, as we find that the Ni induces substantial distortions within the W(110) surface layer, with lateral displacements of the W atoms as large as 0.3 Å, see Fig. 6d [27]. This substantial Ni-induced distortion has escaped previous investigations and these structural details will be an important ingredient for future stress calculations.

Finally, we discuss briefly the decisive role of even small strain in the sub-percent range for the modified magneto-elastic coupling and magnetic anisotropy of epitaxial thin films as compared to their bulk counterparts.

6 Magneto-elastic Coupling: Non-bulk-like Behavior in Epitaxial Films

The coupling between lattice strain and magnetic anisotropy energy is given by the magneto-elastic coupling. This effect can be understood as the strain dependent part of the magnetic anisotropy energy density. The magneto-elastic coupling takes the empirical result into account which indicates that ferromagnetic samples change their length upon magnetization. For Fe this effect is quite small, the strain induced by the magnetization along [100] amounts only to 2×10^{-5}, measured along [100], starting from a demagnetized state. This effect is called magnetostriction. Ferromagnetic films have also the tendency to strain upon magnetization changes. But they are bonded rigidly

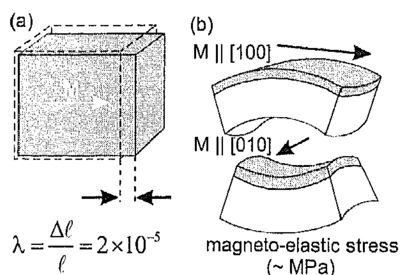

Fig. 7. (**a**) Magnetostriction of a bulk sample leads to a strain λ. (**b**) The same effect, namely the magneto-elastic coupling, leads to a stress in the film, which induces an anticlastic curvature of the substrate

to a substrate, and magneto-elastic stresses (also: magnetostrictive stresses) are induced instead. The degree of resulting film-substrate deformation depends on the rigidity of the substrate. Figure 7 shows the difference between magnetostriction of a bulk sample and magnetostrictive stress in a film.

The important aspect of magneto-elastic coupling is that the stress state of ferromagnetic film can be changed by changing the orientation of the film magnetization. A measurement of the change of curvature upon reorientation of the magnetization reveals the magnitude of the effective magneto-elastic coupling.

Therefore, highly sensitive stress measurements are appropriate to measure magneto-elastic coupling coefficients, provided that the sensitivity is sufficient to detect stress changes which are often three orders of magnitude smaller (MPa) as compared to epitaxial misfit stress (GPa). The orientation of the crystal axes, the magnetization directions and of the curvature measurement determine which coupling coefficient is measured. The appropriate data evaluation is discussed in [7,18]. E.g., switching the magnetization direction between the in-plane [100] and [010] direction of a cubic film and measuring the curvature along the [100] direction gives access to B_1.

Combined stress measurements during film growth and magneto-elastic stress measurements reveal the impact of film strain on the effective magneto-elastic coupling. According to the measurements, the effective magneto-elastic coupling varies with film thickness. Therefore, at first sight one might be tempted to ascribe the variation of B_i to a thickness effect. However, the stress measurements reveal, that also the film stress varies with film thickness, and consequently the film strain is expected to vary with the film thickness [33]. It has been possible to produce films of equal thickness but different strain by lightly modifying the growth parameters during film deposition [34]. These measurements, and our own measurements of the magneto-elastic coupling coefficients, clearly indicate a strain-dependent correction of the effective magneto-elastic coupling coefficients.

In Fig. 8a we present a plot of the stress as a function of Fe thickness for different experiments on Fe growth on W(001). The plots Fig. 8b–e show the effective magneto-elastic coupling B_{eff} for Fe [7], Co [35], Ni [36] and Fe on Cu(001) [36]. For Fe on Cu a combination of B_1 and B_2 is measured [36]. The

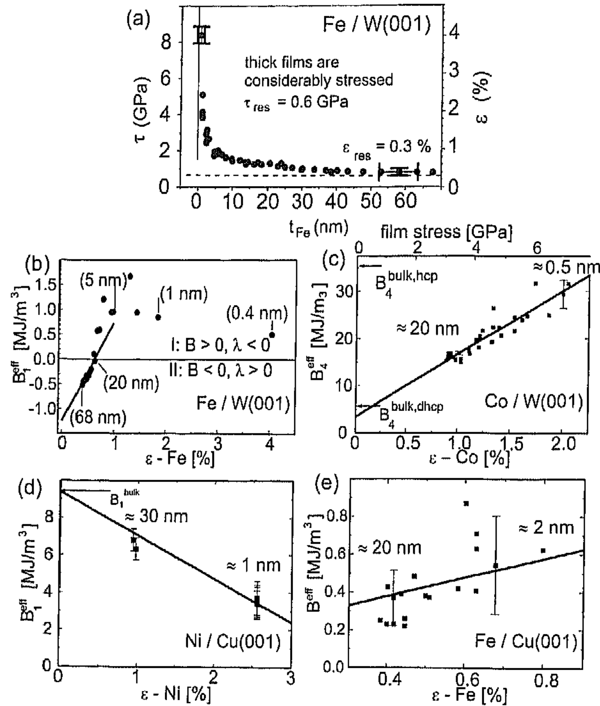

Fig. 8. (a) Film stress for Fe on W(001). Note the considerable residual stress even in thicker films. (b)–(e) The effective magneto-elastic coupling constants B_{eff} of various systems. The *straight lines* through the data points indicate a strain-dependent modification of B_{eff}

straight lines through the data points indicate a modification of the effective magneto-elastic coupling constants in proportion to film strain.

The modified magneto-elastic coupling has an important impact on the magnetic anisotropy of strained films. Although magnetostriction of bulk Fe is a small effect, the underlying magneto-elastic coupling gives rise to an important contribution to the magnetic anisotropy of strained films. The reason is the larger magnitude of the coupling constants B ($B_1(\text{Fe}) = -3.44\ \text{MJ/m}^{-3}$) as compared to the crystalline anisotropy K, ($K_1(\text{Fe}) = 0.05\ \text{MJ/m}^{-3}$). This values correspond to an energy per atom of the order of 0.3 meV for the former, and 4 μeV for the latter [7,37]. The magneto-elastic coupling coefficient B_1 couples the strain ϵ to the energy density via a term $\sim B_1\epsilon$, thus even a strain in the percent range renders the magneto-elastic coupling a decisive contribution to the magnetic anisotropy.

Therefore, measurements of the magneto-elastic coupling are mandatory to put the anisotropy discussion of strained films on a physically sound foundation. The most important result of all experimental determinations of the

various B_i of different epitaxially strained systems indicate that magnitude and sign of B_i are not given by the respective bulk value [7]. Instead, the data analysis suggests that the effective B_i is given by a strain dependent correction of the bulk value. This important result was not considered in earlier anisotropy discussions.

Recently, a strain dependent correction of the magneto-elastic coupling was also found in state-of-the-art calculations of the strain dependence of the magnetic anisotropy [38,39,40,41,42,43]. We conclude that non-bulk like magneto-elastic coupling is a general phenomenon in epitaxially strained films, and the application of bulk coupling constants to anisotropy problems will lead to erroneous results.

7 Conclusion and Outlook

Although stress measurements on thin films have a tradition which dates back to the 1850's, highly sensitive experiments reveal exciting new results, which cannot be ascribed to simple stress-strain relations. Stress in the (sub)-monolayer coverage range are determined by the often strong adsorbate-substrate interaction which can induce substantial distortions or intermixing at the interfaces. The electronic origins of the corresponding stress changes are still under debate and are a topic of current research [8,44].

New insight into the correlation between even subtle structural relaxations and forces acting in film-substrate composite is accessible by combined stress and surface X-ray diffraction measurements. Here, ab initio based calculation can elucidate the relevant mechanisms on the mesoscale [45,46].

The effect of even relatively small strains in the sub-percent range on the magnetic anisotropy of thin films are profound. The implication for the application of nanometer thin films in sensors are significant. Recent first principles calculations support convincingly the experimental result of a strain-induced modification of the magneto-elastic coupling [42]. Further work on alloys should investigate the consequences for technologically relevant systems.

Acknowledgements

The authors thank the E.S.R.F. for support and assistance during the experiments performed at beamline ID-3. We thank Heike Menge from the MPI Halle for the skillful preparation of high quality thin crystalline substrates and Fe whiskers.

References

1. R.W. Hoffman, Phys. Thin Films **3**, 211 (1966).
2. M. F. Doerner and W.D. Nix, CRC Crit. Rev. Solid State and Materials Science **14**, 225 (1988).

3. W.D. Nix, em Metall. Trans. A **20A**, 2217 (1989).
4. G.G. Stoney, Proc. R. Soc. London A **82**, 172 (1909).
5. M.S. Hu, M.D. Thouless, and A.G. Evans, Acta metall. **36**, 1301 (1987).
6. W. Wulfhekel, F. Zavaliche, F. Poratti, H.P. Oepen, and J. Kirschner, Europhys. Lett. **49**, 651 (2000).
7. D. Sander, Rep. Prog. Phys. **62**, 809 (1999).
8. H. Ibach, Surf. Sci. Rep. **29**, 193 (1997).
9. W.D Nix and B.M. Clemens, J. Mater. Res. **14**, 3467 (1999).
10. D. Sander and H. Ibach, in: *Landolt-Börnstein, Numerical Data and Functional Relationships in Science and Technology, New Series, Group III: Condensed Matter*, Volume 42, A 2, H. Bonzel, ed.; Springer, Berlin (2002).
11. D. Sander, Curr. Opinion Solid St. Mat. Sci. **1**, 51 (2003).
12. L.H. He and C.W. Lim, em Surf. Sci. **478**, 203 (2001).
13. V. Buck, Z. Physik B, **33**, 349 (1979).
14. M. Moske, PhD thesis, Georg-August Universität Göttingen, Mathematisch-Naturwissenschaftliche Fachbereiche (1988).
15. M. Weber, R. Koch, and K.H. Rieder, Phys. Rev. Lett. **73**, 1166 (1994).
16. D. Sander, S. Ouazi, V.S Stepanyuk, D.I. Bazhanov, and J. Kirschner, Surf. Sci. **512**, 281 (2002).
17. K. Dahmen, S. Lehwald, and H. Ibach, Surf. Sci. **446**, 161 (2000).
18. K. Dahmen, H. Ibach, and D. Sander, J. Magn. Magn. Mater. **231**, 74 (2001).
19. R. Mahesh, D. Sander, , S.M. Zharkov, and J. Kirschner, Phys. Rev. B **68**, 0454XX (2003).
20. A. Enders, PhD thesis, Martin-Luther Universität Halle-Wittenberg, Mathematisch-Naturwissenschaftlich-Technische Fakultät (1999).
21. Th. Gutjahr-Löser. PhD thesis, Martin-Luther Universität Halle-Wittenberg, Mathematisch-Naturwissenschaftlich-Technische Fakultät (1999).
22. Klaus-Thomas Wilke. *Kristallzüchtung.* Dt. Verl. d. Wiss., Berlin (1988).
23. B. Heinrich, K.B. Urquhart, J.R. Dutcher, S.T. Purcell, J.F. Cochran, A.S. Arrot, D.A. Steigerwald, and W.F. Egelhof, Jr., J. Appl. Phys. **63**, 3863 (1988).
24. J. Unguris, R.J. Celotta, and D.T. Pierce, J. Magn. Magn. Mater. **127**, 205 (1993).
25. P. Gumbsch and M.S. Daw, Phys. Rev. B **44**, 3934 (1991).
26. J. Massies and N. Grandjean, Phys. Rev. Lett. **71**, 1411 (1993).
27. H.L. Meyerheim, D. Sander, R. Popescu, J. Kirschner, O. Robach, S. Ferrer, and P. Steadman, Phys. Rev. B **67**, 155422 (2003).
28. H.L. Meyerheim, D. Sander, R. Popescu, J. Kirschner, and S. Steadman, P.and Ferrer, Phys. Rev. B **64**, 045414-1 (2001).
29. H.L. Meyerheim, D. Sander, R. Popescu, S. Steadman, P.and Ferrer, and J. Kirschner, Surf. Sci. **475**, 103 (2001).
30. R. Popescu, H.L. Meyerheim, D. Sander, J. Kirschner, P. Steadman, O. Robach, and S. Ferrer, Phys. Rev. B. submitted, (2003).
31. D. Sander, C. Schmidthals, A. Enders, and J. Kirschner, Phys. Rev. B **57**, 1406 (1998).
32. C. Schmidthals, D. Sander, A. Enders, and J. Kirschner, Surf. Sci. **417**, 361 (1998).
33. J.W. Matthews and J.L. Crawford, Thin Solid Films **5**, 187 (1970).
34. G. Wedler, J. Walz, A. Greuer, and R. Koch, Phys. Rev. B **60**, R11313 (1999).
35. Th. Gutjahr-Löser, D. Sander, and J. Kirschner, J. Magn. Magn. Mater. **220**, L1 (2000).

36. Th. Gutjahr-Löser, D. Sander, and J. Kirschner, J. Appl. Phys. **87**, 5920 (2000).
37. P. Bruno, in: *Magnetismus von Festkörpern und Grenzflächen*, Physical origins and theoretical models of magnetic anisotropy, pages 24.1–24.28. Forschungszentrum Jülich, Jülich (1993).
38. M. Komelj and M. Fähnle, J. Magn. Magn. Mater. **220**, L8 (2000).
39. M. Komelj and M. Fähnle, Phys. Rev. B **65**, 092403–1 (2002).
40. M. Komelj and M. Fähnle, J. Magn. Magn. Mater. **238**, L125 (2002).
41. M. Komelj and M. Fähnle, Phys. Rev. B **65**, 212410–1 (2002).
42. M. Fähnle, M. Komelj, R.Q. Wu, and G.Y. Guo, Phys. Rev. B **65**, 144436–1 (2002).
43. M. Fähnle and M. Komelj, J. Magn. Magn. Mater. **220**, L13 2000.
44. J.E. Müller, K. Dahmen, and H. Ibach, Phys. Rev. B **66**, 235407–1 (2002).
45. V.S. Stepanyuk, D.A. Bazhanov, A.N. Baranov, W. Hergert, P.H. Dederichs, and J. Kirschner, Phys. Rev. B **62**, 15398 (2000).
46. O.V. Lysenko, V.S Stepanyuk, W. Hergert, and J. Kirschner, Phys. Rev. Lett. **89**, 126102–1 (2002).